Bottom-Reflector Enhanced Grating Couplers Micro-Transfer Printed on Silicon Nitride Photonic Integrated Circuits

Zuyang Liu , Jing Zhang , Gunther Roelkens , *Senior Member, IEEE*, Nicolas Le Thomas , and Roel Baets , *Life Fellow, IEEE*

Abstract—We demonstrate a new post-processing approach to efficiently couple light in silicon nitride (Si_3N_4) photonic integrated circuits (PIC) via grating couplers add-ons. Thin-film coupons of apodised Si_3N_4 grating couplers enhanced with metallic bottom reflectors and adiabatic couplers are micro-transfer printed onto the input and output of Si_3N_4 waveguides, providing efficient coupling without impacting the rest of the PIC. Two-dimensional FDTD simulations predict coupling efficiencies as large as 62.4% (-2.0 dB) at a wavelength of 785 nm with a coupling optical fiber tilted at $10°$. As a proof-of-concept, we report an experimental coupling efficiency of -2.1 dB which is 3 dB better than the value obtained with standard designs of grating couplers.

Index Terms—Grating couplers, integrated optics, micro-transfer-printing, silicon nitride.

I. INTRODUCTION

SILICON nitride (Si_3N_4) has become a widely exploited material for integrated photonics [1]. Its low loss and transparency in the near-infrared and visible range benefit emerging applications such as biosensing [2], telecommunication [3], and quantum computing [4]. Furthermore, Si_3N_4 is compatible with complementary metal-oxide-semiconductor (CMOS) fabrication processes, enabling large-scale manufacturing. However, efficient coupling of light between high index contrast Si_3N_4 waveguides and optical fibers remains challenging due to a mismatch between the mode area. Grating couplers are commonly employed to facilitate vertical coupling of light between on-chip waveguides and optical fibers. With periodic structures etched into the guiding layer, light propagating in the waveguide can be diffracted upwards toward an optical fiber, and vice versa. Compared to horizontal coupling using edge couplers, vertical coupling with grating couplers are more flexible in on-chip position and less sensitive to optical alignment.

Si_3N_4 grating couplers are generally less efficient than their silicon-on-insulator (SOI) counterparts because of the lower index contrast between Si_3N_4 and SiO_2 than that between Si and SiO_2. The scattering strength of each pitch is lower. And the grating period is larger, resulting in fewer scattering elements in a given fiber diameter. Therefore, the power that can be coupled to an optical fiber is lower. We aim to optimize the coupling of the scattered light into an optical fiber for an integrated platform operating in the visible and near-infrared wavelength range.

One approach to improve the coupling efficiency of grating couplers consists in incorporating a bottom reflector beneath the grating. It prevents leakage towards the bottom substrate, which is the main origin of coupling loss. By carefully adjusting the distance between the grating and the bottom reflector, constructive interference between the light directly coupled and reflected into the grating can be achieved for a target wavelength. Different types of bottom reflectors have been investigated, including single-layer metal reflectors, distributed Bragg reflectors, reflection gratings, etc. Coupling efficiencies as high as -1 dB have been demonstrated numerically and experimentally [5], [6], [7]. However, these reflectors introduce additional fabrication complexity, leading to incompatibility with standard waveguide platforms. It increases the cost and time to integrate such components in mass production.

This paper introduces micro-transfer printed (μTP) Si_3N_4 grating couplers, offering a scalable and cost-effective solution for efficient coupling on standard Si_3N_4 platforms. Micro-transfer printing is a versatile technology that enables heterogeneous integration with high throughput and efficient use of heterogeneous materials [8]. It has been widely employed in the integration of lasers [9], [10], [11], amplifiers [12], modulators [13], [14], photodetectors [15], [16], [17], etc. Using this technology, the grating couplers and metal reflectors are fabricated separately and later transferred onto the target photonic integrated circuit (PIC). Assisted by the bottom reflector and an apodised grating, an efficient coupling can be realized without modifying the rest of the PIC with complex processing steps. It also creates more opportunities for the supply chain of PICs by adding the grating couplers in a late stage of the fabrication flow.
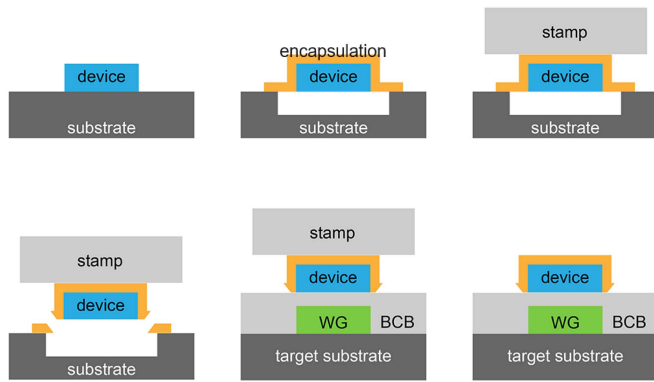
Fig. 1. Process of micro-transfer-printing technology: pre-fabrication, release, and transfer. The encapsulation layer can be formed by photoresist, oxide, or other dielectric materials.
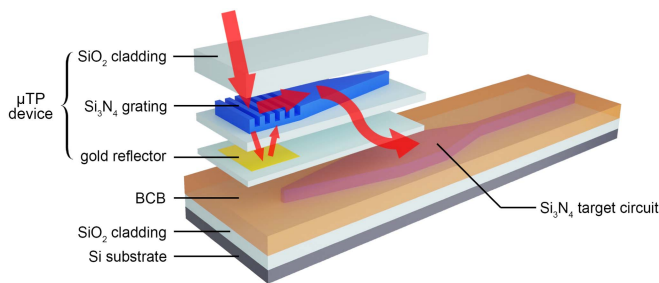

Fig. 2. Schematics of the μTP Si$_3$N$_4$ grating coupler with a gold bottom reflector on a target circuit. Dimensions are not to scale. Red arrows represent the flow of light as an in-coupling device.

In this paper, we first discuss the working principle and simulation results of the proposed grating coupler, followed by a brief explanation of the fabrication process. Then the measurement results are presented and we finally conclude.

II. PRINCIPLE AND SIMULATION

Micro-transfer-printing starts with the fabrication of devices densely positioned on a source wafer. Then they are released and transferred to a target wafer using an adhesive polydimethyl-siloxane (PDMS) stamp. Fig. 1 shows schematically the process. Multiple devices can be transferred in parallel using a patterned stamp, which allows scaling out from dense array of devices to sparse positions on target circuits. The printing cycle takes down to 30 seconds. Compared to flip-chip and bonding, its use of source material is more efficient, and different source materials can be integrated more densely on the target wafer.

The proposed grating coupler is illustrated in Fig. 2. The Si$_3$N$_4$ grating and the gold reflector are separated by a thin layer of SiO$_2$ and sandwiched between top and bottom SiO$_2$ cladding. The grating has a width of 5 μm to match the core diameter of single-mode optical fibers at 785 nm. When light is coupled into the circuit through the grating coupler, the downward-diffracted light is reflected by the gold reflector and coupled back into the silicon nitride layer. By carefully adjusting the vertical distance between the reflector and the grating, the reflected and directly coupled light interfere constructively. The grating couplers with
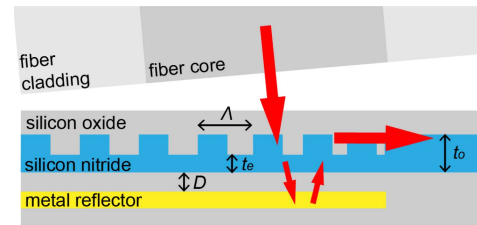

Fig. 3. Sketch of the cross-section of the apodised grating. Red arrows represent the flow of light as in-coupling device.

bottom reflectors are fabricated on a separate wafer, released by locally under-etching the device, and transferred onto a target circuit on another wafer with a layer of Si$_3$N$_4$ on top of buried oxide and Si substrate. There are two tapers, one in micro-transfer printed structure and the other on the target integrated circuit. Both tapers have the same geometry but are in opposite directions, thus forming an adiabatic coupler for efficient light coupling between two Si$_3$N$_4$ layers. Compared to directional couplers, adiabatic couplers achieve the same efficiency with more extensive lengths while being more tolerant to variations in layer thicknesses, refractive indices, and coupler length. The adhesion of the source device is improved by a thin layer of benzocyclobutene (BCB) with a typical thickness of 50 nm.

The coupling efficiency is boosted mainly by the bottom reflector. Additionally, the gratings are apodised to further improve the efficiency. Regular grating couplers have a constant pitch and fill factor, leading to a constant coupling strength and an exponentially decaying out-coupling power. It has a considerable mismatch with the Gaussian mode of optical fibers. By varying the fill factor and the period along the propagation direction in the waveguide, the out-coupling power can be tailored more Gaussian-like. In this work, we adapt the method presented by Marchetti et al. [18]. The fill factor F is linearly varied along the grating as

$$F = F_0 - R \cdot z \tag{1}$$

where F_0 is the initial fill factor at the start of the grating. R is the varying rate of the fill factor, and z is the distance from the grating input. The initial fill factor is set to 0.9 to mitigate the abrupt change of optical impedance and reduce scattering. It has been shown that a fill factor of 0.5 gives rise to the highest out-coupling power [19]. Therefore, the out-coupling power is lowered at the grating input. Once the fill factor is reduced to 0.5 along the propagation direction, it stays at this value afterward to diffract out as much power as possible. The cross-section of the grating is sketched in Fig. 3.

The diffraction angle is given by

$$\sin \theta = n_{eff} - \frac{\lambda_c}{\Lambda}. \tag{2}$$

Where the grating is apodised, the effective index changes with the fill factor. Therefore, to maintain the same diffraction angle θ, the period Λ should be varied accordingly as

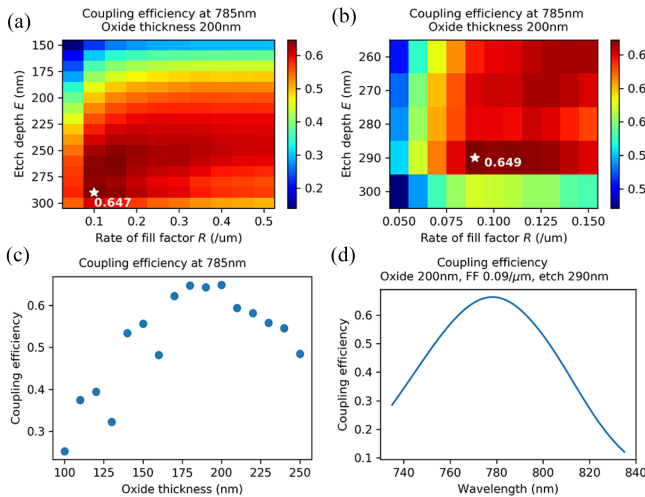$$\Lambda = \frac{\lambda_c}{n_{eff}(z) - \sin \theta}. \tag{3}$$

Fig. 4. Estimated coupling efficiency with 10°-tilted fiber. (a) A coarse sweep of R and E. (b) A fine sweep of R and E. (c) A sweep of oxide thickness between the metal reflector and the grating. (d) The coupling efficiency of the optimal design.

The effective index n_{eff} of each pitch is estimated as

$$n_{eff}(z) = F \cdot n_o + (1 - F) \cdot n_e \qquad (4)$$

where n_o and n_e are the effective indices of waveguides with a thickness of t_o and t_e, respectively. These effective indices are determined numerically.

Apart from the grating and bottom reflector, the adiabatic coupler between the two Si₃N₄ layers also contribute to the overall coupling efficiency. To reduce the complexity and running time, the two parts are evaluated separately in the simulation.

The grating is defined by several parameters. The varying rate R of the fill factor along the propagation direction tailors the output profile. The out-coupled power is also affected by the etch depth $E = t_o - t_e$. Moreover, the oxide thickness D between grating and reflector determines the optimal wavelength for achieving a constructive interference effect. Besides R, E, and D, the fiber angle θ and position of the optical fiber have to be optimized. The grating coupler is evaluated as an in-coupling device in two dimensional (2D) simulations using Lumerical FDTD solutions.

Using ellipsometry on Si₃N₄ thin films deposited via plasma-enhanced chemical vapor deposition (PECVD), the Si₃N₄ material has a refractive index of 1.93 around the target wavelength of 785 nm. The thickness of Si₃N₄ is 300 nm on the micro-transfer printed device and the target circuit. The value of the refractive index of SiO₂ is measured to be around 1.44. The reflector is assumed for the simulation to be a 50 nm-thick gold patch.

The fiber angle is set at 10°. As an initial guess, the oxide thickness is chosen as 200 nm considering the target wavelength and fiber angle. The optimization starts from a crude sweep of R and E. Fig. 4(a) shows the numerically calculated coupling efficiency. The fiber position is swept simultaneously for each combination of R and E. Only the results from optimal fiber positions are displayed. Then a fine sweep is performed around
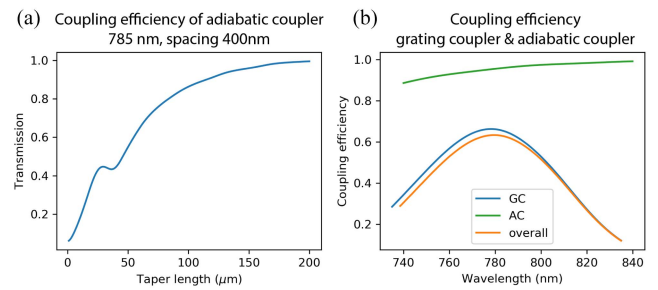

Fig. 5. (a) Estimated coupling efficiency of adiabatic couplers with varied taper lengths. (b) Estimated coupling efficiency of the grating coupler (GC), 150 μm long adiabatic coupler (AC), and the overall coupling efficiency of the μTP grating coupler.

the optimal combination of the first parameter sweep. The results are presented in Fig. 4(b), from which the final optimal combination is found at $R = 0.09\ \mu m^{-1}$ and $E = 290$ nm.

Then the oxide thickness D is swept from 100 nm to 250 nm while sweeping the fiber position. For each value of D, the optimal coupling efficiency is included in Fig. 4(c). The highest power coupling efficiency is reached when the oxide thickness is 200 nm. For this grating coupler design with $R = 0.09\mu m^{-1}$, $E = 290$ nm and $D = 200$ nm, the coupling efficiency for a wavelength range from 740 nm to 840 nm is numerically estimated as shown in Fig. 4(d). The coupling efficiency is 64.9% (-1.88 dB) at the wavelength of 785 nm. The 1-dB bandwidth is 44 nm.

The coupling efficiency from the micro-transfer printed device to the target circuit is also affected by the adiabatic coupler. The adiabatic coupler consists of two tapers separated vertically, positioned in opposite directions. The effective index gradually changes in both layers along the propagation direction. The coupling efficiency is determined by the taper length and the vertical spacing. The latter includes the oxide thickness D, reflector thickness, bottom thickness on the source, BCB thickness, and top cladding thickness on the circuit. From previous experiments, the BCB thickness after printing is known to be around 50 nm for the type and dilution in use. Bottom and top oxide cladding thicknesses are set to 50 nm. The gold reflector is assumed to have a thickness of 50 nm. Therefore the total spacing is 400 nm including the optimal oxide thickness $D = 200$ nm from previous simulations. The two identical trapezoid tapers have base widths of 5 μm and 0.15 μm. The coupling efficiency for varied taper lengths is estimated as in Fig. 5(a) using EME (eigenmode expansion) solver in Lumerical MODE solutions. It requires a minimum length of 150 μm to achieve a coupling efficiency of 96% at the wavelength of 785 nm. The coupling efficiency of 150 μm long adiabatic couplers is shown in Fig. 5(b), together with that of the grating coupler and the overall structure. The overall efficiency at 785 nm is 62.4% (-2.0 dB) for a fiber angle of 10°.

Misalignment between the tapers may occur during μTP in translational or rotational manners. The effect of lateral misalignment relative to the propagation direction on the coupling efficiency of the 150 μm long adiabatic coupler is presented in Fig. 6. With a misalignment up to 0.6 μm, the change in
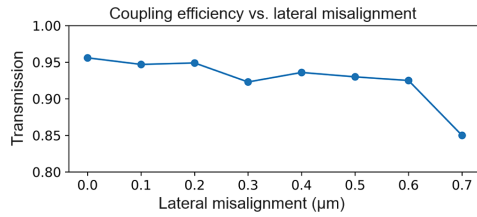
Fig. 6. Estimated coupling efficiency of 150 μm long adiabatic couplers with varied misalignment perpendicular to the propagation direction.

coupling efficiency is negligible. Misalignment in the other translational direction along the propagation direction of light is rather tolerant because of the length of the tapers. Rotational misalignment is not studied in depth in this paper, but it is expected to be small and relatively tolerant in adiabatic couplers.

III. FABRICATION

The fabrication process of source devices is shown in Fig. 7. It starts by depositing 180 nm SiO $_2$ on a bare silicon (Si) sample using PECVD. The purpose of this oxide layer is to separate the gold patch from the Si substrate, protect it during release, and support it afterward. Then a recess with the same size and depth as the reflector is etched in the oxide layer using UV contact lithography and reactive ion etching (RIE), and a layer of gold is deposited using a metal evaporator. The depth of the recess and the thickness of the gold is 80 nm to ensure efficient reflection. The gold reflectors are then defined through metal lift-off by immersing the sample in acetone to remove the photoresist and gold on top. It leaves only materials in the recess, forming a flat top surface. Gold alignment markers are defined in this step as well for the alignment among following lithography steps of gratings, tapers, and coupons. To improve the adhesion between gold and SiO$_2$, titanium layers of a few nanometers are deposited before and after the gold deposition. The next step consists in a layer of SiO$_2$ being deposited via PECVD. It is followed by the deposition of the guiding layer of 300 nm-thick Si$_3$N$_4$ via PECVD as well. To improve alignment accuracy, the Si$_3$N$_4$ and SiO $_2$ are removed on top of the markers. The shallow-etched gratings and deep-etched tapers are then defined by two separate steps of electron beam lithography (EBL) and RIE. To fill the grating lines and planarize the top surface, hydrogen silsesquioxane (HSQ) is spun onto the sample and cured at 400 $^\circ$ C. HSQ is an inorganic compound usually used as a resist in photolithography and EBL. When heated to 400°C, the polymer forms a three-dimensional network of silsesquiox-ane and silicon-rich oxide, providing mechanical integrity and chemical resistance to the subsequent processing [20]. Finally, a 100 nm-thick layer of SiO$_2$ is deposited via PECVD.

The release process begins with a deep, dry etching around the coupons into the Si substrate. The sample is immersed in 5% tetramethylammonium hydroxide (TMAH), which etches the Si substrate with high selectivity against SiO$_2$ [21]. After the under-etching of the Si substrate, the coupons are ready for micro-transfer-printing. The coupons are kept suspended by tethers formed by the deposited layers where they were not etched during the deep etching.

The target sample also starts from a bare Si substrate. After depositing 3 μm of SiO $_2$ and 300 nm of Si$_3$ N$_4$ with PECVD, waveguides with adiabatic tapers are etched in the Si$_3$N$_4$ layer using EBL and RIE. Before μTP, a thin layer of BCB (4022-35, diluted 1:3 using mesitylene) is spun onto the target sample at 3000 rpm for 40 seconds. It is later heated at 150 $^\circ$C for 15 minutes to accelerate the evaporation of the solvent mesitylene and slightly cure the layer to prevent subsequent flowing. The BCB thickness is around 150 nm before printing the coupons onto the ends of the waveguides. The BCB thickness is reduced to 50 nm beneath the coupon after printing. Fig. 8 shows μTP grating couplers printed onto a target sample, observed with an optical microscope.

IV. MEASUREMENTS

To characterize the coupling efficiency of the μTP grating couplers printed onto Si$_3$N$_4$ waveguides, the coupling loss of the grating coupler and the adiabatic couplers are treated as a whole. Light with a wavelength from 780 nm to 880 nm is coupled into the waveguide through a single-mode optical fiber tilted at 10° with a mode field diameter of 5 μm and later extracted via a second nominally identical grating coupler. We first measure the insertion loss of waveguides with μTP grating couplers on both ends.

The insertion loss consists of the coupling loss at the two ports and the propagation loss. The propagation loss is estimated from the change of scattered intensity along the waveguide. It is recorded by a camera imaging the sample surface. A typical image of the scatted intensity of the propagating light field is included in Fig. 9. The decay rate of the intensity along the waveguide represents the propagation loss of the waveguide. The periodic peaks in Fig. 9 correspond to the stitching error resulting from the electron beam lithography, which are 500 μm apart. Measuring three waveguides on the sample results in an average propagation loss of 8.5±0.3 dB/cm for 300-nm thick, 800-nm wide, low-frequency PECVD Si$_3$N$_4$ waveguides.

The grating couplers are printed onto a series of waveguides with lengths of 7, 8, and 9 mm. An average coupling efficiency is obtained between the two grating couplers on one waveguide by subtracting the corresponding propagation loss from the total insertion loss. Fig. 10 shows the best coupling efficiency measured with common and μTP grating couplers. The common grating couplers are fabricated on 300 nm Si$_3$N$_4$ on top of 3 μm buried oxide on a Si substrate without micro-transfer printing or metal reflectors. They have an etch depth of 300 nm, a period of 610 nm and a constant fill factor of 0.5. The μTP grating couplers have an etch depth of 230 nm and a fill factor variation rate of 0.11 μm $^{-1}$. The fabricated combinations of D and R is different from the theoretical optimal combination for 10° fiber. When the fill factor reaches 0.5, the pitch is 616 nm. Six nominally identical devices are printed onto three identical waveguides. The colored dots in Fig. 10 show the coupling efficiency averaged between two devices on each waveguide. As a comparison, we include the measured coupling efficiency of standard grating
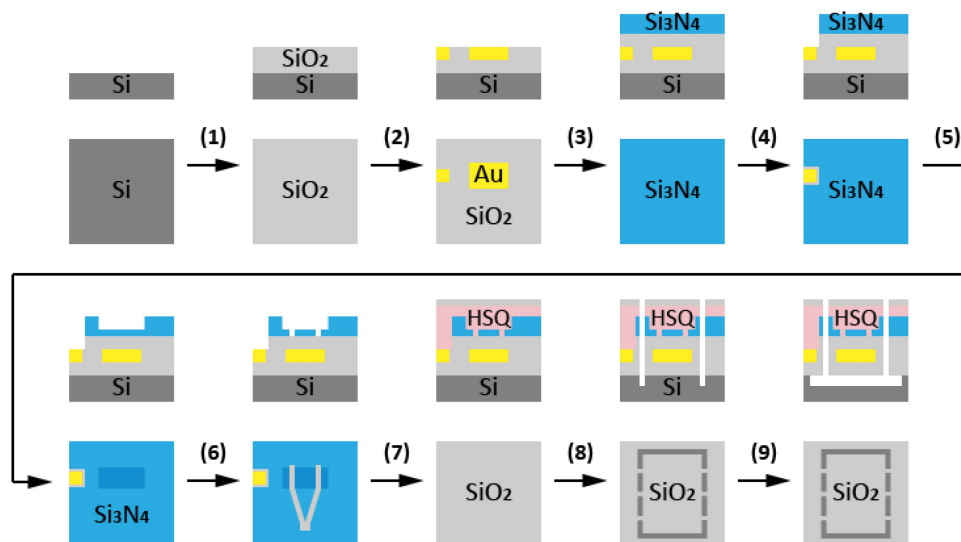
Fig. 7.   Process flow of coupons of coupon patterning and release. Cross-section and top-view are shown for each step.
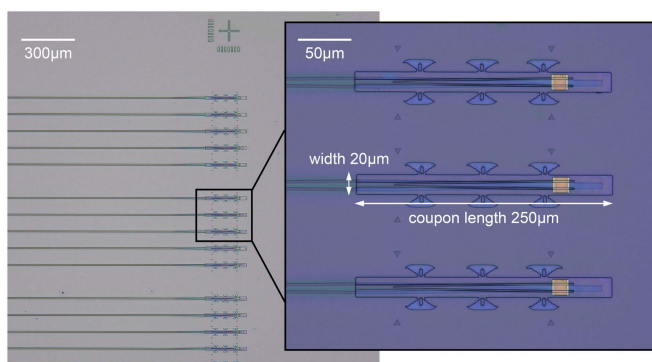

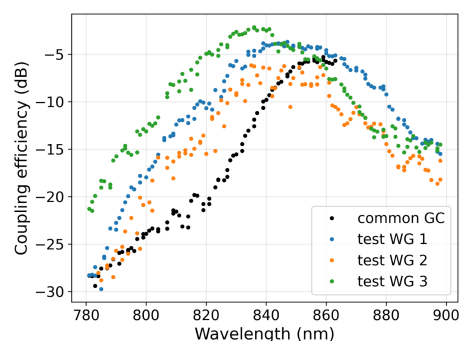Fig. 8.   Grating couplers printed onto a target sample.

Fig. 10.   Coupling efficiency of μTP and common grating couplers in the wavelength range from 780 to 880 nm.

the wavelength of 840 nm, while the average efficiency on the three waveguides is -4.0 dB. The discrepancy could be induced by misalignment and small variations in fabrication quality. The maximum and average coupling efficiency are both 3 dB better than the efficiencies measured with the common grating couplers, which complies with the numerical simulation.

Note that the center wavelength is shifted by over 50 nm compared to the design. The properties of Si_3N_4 and SiO_2 are slightly different from the simulation. It affects the effective index of the grating and the effective distance between the grating and the reflector. Finally, uncertainties in other properties, such as HSQ thickness and index, may also affect the center wavelength and efficiency.

The main application envisioned for the proposed process flow is to achieve higher coupling efficiency to silicon nitride waveguides. But there are other applications as well: the method allows to decouple the technology needed for the silicon nitride PICs from the one needed for the bottom-reflector enhanced grating couplers, thereby creating more supply chain options for manufacturing these devices. Furthermore, the addition of grating couplers in a late stage of the manufacturing can be seen
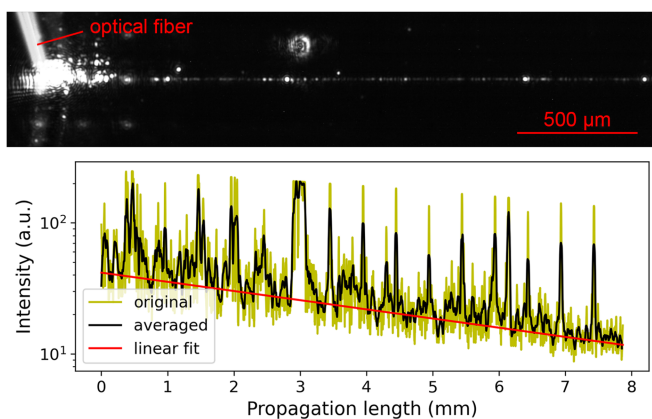

Fig. 9.   Above: camera pictures of light scattered by the waveguide. Below: the scattered light intensity along the waveguide.

couplers (black dots in Fig. 10), which are fully etched on the input and output of the waveguides with a pitch of 610 nm and a fill factor of 0.5. The highest coupling efficiency of the μ TP grating couplers is found as high as -2.1 dB around

as a form of programmability of the circuit. A generic circuit can be turned into a variety of different devices by adding grating couplers in different locations. Finally by adjusting the coupling efficiency of the adiabatic coupler, signal probing can be realized via a post-processed addition of functionality. Probing can be useful to debug a complex circuit. It can also be used to serve a feedback loop that adjusts the properties of one of the on-chip devices (e.g. tune a ring resonator). Thanks to the high coupling efficiency of the grating, the impact on the propagating signal can be kept to a minimum.

V. CONCLUSION

In this manuscript, we demonstrate a micro-transfer-printed Si_3N_4 grating coupler that can boost the light coupling efficiency on Si_3N_4 PIC-platforms. The coupling efficiency improvement is mainly due to a metallic bottom reflector and the apodization of the grating. Thanks to the micro-transfer printing technology, metallic bottom reflectors can be introduced without modifying the standard process flow of an existing platform are not necessary when applying such grating couplers. Designing of the grating coupler begins with numerical optimization of the grating parameters and layer thicknesses for the wavelength of 785 nm. The coupling efficiency can reach -2.0 dB at a wavelength of 785 nm from simulations. The best experimental coupling efficiency reaches a value of -2.1 dB at a wavelength of 840 nm, while the average efficiency over nominally identical devices is -4.0 dB, both 3 dB better than conventional grating couplers fabricated on the same wafer. It significantly increases the coupling efficiency on standard Si_3N_4 platforms, creates more options for the manufacturing supply chain and allows to implement new functionalities for generic circuits.

ACKNOWLEDGMENT

REFERENCES

[1] A. Rahim et al., "Expanding the silicon photonics portfolio with silicon nitride photonic integrated circuits," *J. Lightw. Technol.*, vol. 35, no. 4, pp. 639–649, Feb. 2017.

[2] A. Z. Subramanian et al., "Silicon and silicon nitride photonic circuits for spectroscopic sensing on-a-chip," *Photon. Res.*, vol. 3, no. 5, pp. B47–B59, 2015.

[3] D. J. Blumenthal, R. Heideman, D. Geuzebroek, A. Leinse, and C. Roelofzen, "Silicon nitride in silicon photonics," *Proc. IEEE*, vol. 106, no. 12, pp. 2209–2231, Dec. 2018.

[4] A. W. Elshaari, W. Pernice, K. Srinivasan, O. Benson, and V. Zwiller, "Hybrid integrated quantum photonic circuits," *Nature Photon.*, vol. 14, pp. 285–298, 2020.

[5] S. Romero-Garcia, F. Merget, F. Zhong, H. Finkelstein, and J. Witzens, "Visible wavelength silicon nitride focusing grating coupler with AlCu/TiN reflector," *Opt. Lett.*, vol. 38, no. 14, pp. 2521–2523, 2013.

[6] H. Zhang et al., "Efficient silicon nitride grating coupler with distributed bragg reflectors," *Opt. Exp.*, vol. 22, no. 18, pp. 21800–21805, 2014.

[7] J. Zou, Y. Yu, M. Ye, L. Liu, S. Deng, and X. Zhang, "Ultra efficient silicon nitride grating coupler with bottom grating reflector," *Opt. Exp.*, vol. 23, no. 20, pp. 26305–26312, 2015.

[8] G. Roelkens et al., "Present and future of micro-transfer printing for heterogeneous photonic integrated circuits," *APL Photon.*, vol. 9, no. 1, 2024, Art. no. 010901.

[9] J. Goyvaerts et al., "Enabling VCSEL-on-silicon nitride photonic integrated circuits with micro-transfer-printing," *Optica*, vol. 8, no. 12, pp. 1573–1580, Dec. 2021.

[10] B. Haq et al., "Micro-transfer-printed III-V-on-silicon c-band distributed feedback lasers," *Opt. Exp.*, vol. 28, no. 22, pp. 32793–32801, Oct. 2020.

[11] A. Hermans et al., "High-pulse-energy III-V-on-silicon-nitride mode-locked laser," *APL Photon.*, vol. 6, no. 9, 2021, Art. no. 096102.

[12] B. Haq et al., "Micro-transfer-printed III-V-on-silicon C-band semiconductor optical amplifiers," *Laser Photon. Rev.*, vol. 14, no. 7, 2020, Art. no. 1900364.

[13] T. Vandekerckhove et al., "Reliable micro-transfer printing method for heterogeneous integration of lithium niobate and semiconductor thin films," *Opt. Mater. Exp.*, vol. 13, no. 7, pp. 1984–1993, Jul. 2023.

[14] T. Vanackere et al., "Heterogeneous integration of a high-speed lithium niobate modulator on silicon nitride using micro-transfer printing," *APL Photon.*, vol. 8, no. 8, 2023, Art. no. 086102.

[15] J. Goyvaerts et al., "Transfer-print integration of GaAs P-I-N photodiodes onto silicon nitride waveguides for near-infrared applications," *Opt. Exp.*, vol. 28, no. 14, pp. 21275–21285, Jul. 2020.

[16] D. Maes et al., "High-speed uni-traveling-carrier photodiodes on silicon nitride," *APL Photon.*, vol. 8, no. 1, 2023, Art. no. 016104.

[17] S. Cuyvers et al., "Heterogeneous integration of Si photodiodes on silicon nitride for near-visible light detection," *Opt. Lett.*, vol. 47, no. 4, pp. 937–940, Feb. 2022.

[18] R. Marchetti, C. Lacava, L. Carroll, K. Gradkowski, and P. Minzioni, "Coupling strategies for silicon photonics integrated chips," *Photon. Res.*, vol. 7, no. 2, pp. 201–239, 2019.

[19] D. Taillaert et al., "An out-of-plane grating coupler for efficient butt-coupling between compact planar waveguides and single-mode fibers," *IEEE J. Quantum Electron.*, vol. 38, no. 7, pp. 949–955, Jul. 2002.

[20] C.-C. Yang and W.-C. Chen, "The structures and properties of hydrogen silsesquioxane (HSQ) films produced by thermal curing," *J. Mater. Chem.*, vol. 12, pp. 1138–1141, 2002.

[21] J. T. L. Thong, W. K. Choi, and C. W. Chong, "TMAH etching of silicon and the interaction of etching parameters," *Sensors Actuators A*, vol. 63, pp. 243–249, 1997.